

A Switched Systems Framework for Guaranteed Convergence of Image-Based Observers With Intermittent Measurements

Anup Parikh, Teng-Hu Cheng, Hsi-Yuan Chen, and Warren E. Dixon, *Fellow, IEEE*

Abstract—Switched systems theory is used to analyze the stability of image-based observers for three-dimensional localization of objects in a scene in the presence of intermittent measurements due to occlusions, feature tracking losses, or a limited camera field of view, for example. Generally, observers or filters that are exponentially stable under persistent measurement availability may have unbounded error growth under intermittent measurement loss, even while providing seemingly accurate state estimates. By constructing a framework that utilizes a state predictor during periods when measurements are not available, a class of image-based observers is shown to be exponentially convergent in the presence of intermittent measurements if an average dwell time, and a total unmeasurability time, condition is satisfied. The conditions are developed in a general form, applicable to any observer that is exponentially convergent assuming persistent visibility, and utilizes object motion knowledge to reduce the amount of time measurements must be available to maintain convergence guarantees. Based on the stability results, simulations are provided to show improved performance compared to a zero-order hold approach, where state estimates are held constant when measurements are not available. Experimental results are also included to verify the theoretical results, to demonstrate applicability of the developed observer and predictor design, and to compare against a typical approach using an extended Kalman filter.

Index Terms—Computer vision, estimation, range sensing, switched systems, visual tracking.

I. INTRODUCTION

ADVANCES across a spectrum of domains have led to widespread use of imaging systems in robotics applications. Yet, several open problems remain that limit the robustness or stability of imaging systems when used for navigation and visual-servo control. Most of these challenges stem from the

fact that full-state feedback of observed features is not available; three-dimensional (3-D) coordinates are not available due to the projection onto a 2-D image plane (i.e., range to the feature is lost). One method to reconstruct the range information is to use a single camera that acquires multiple overlapping images that can be compared, where the motion of the camera (e.g., in vehicular systems) provides sufficient parallax. This approach is often called structure from motion (SfM).

Recursive techniques for solving the SfM problem have been developed for real-time applications [1]–[7]. These methods formulate a dynamic system to represent the relative motion of an image feature with respect to the camera, and utilize state estimators and observers to reconstruct the Euclidean coordinates of a feature. Observer-based methods have also been applied to the reverse problem of determining feature depth with a stationary camera and known object motion [7]–[12]. In these cases, the feature motion is expressed as an affine dynamical system with partially unmeasurable states, expressed in coordinates relative to the fixed camera. Observers have also been used to recover the relative depth of a moving object from a moving camera with known velocities [13], [14]. In each of these cases, continuous visibility of the object, and hence continuous measurements, is assumed.

A significant issue with using a camera for feedback is the intermittent loss of object visibility [e.g., due to occlusions, feature tracking losses, limited camera field of view (FOV), etc.] and the slow sampling rate (which can be modeled as a periodic loss of object visibility). In this paper, switched systems methods are used to develop an observer–predictor framework and analyze the overall stability of the observer and predictor in the presence of intermittent measurements. The framework is developed in a general way, so that during periods where measurements are available, any exponentially convergent observer can be used to estimate the object position. During periods in which measurements are not available, or in between frames of a video stream, an object motion model is used to extrapolate the position of the object. However, the closed-loop error dynamics during these periods are unstable, and although the estimation error is exponentially stable during the periods in which measurements are available, the estimates may still diverge in the limit if the object is intermittently unmeasurable. By using switched systems theory, sufficient conditions on the measurability time are developed to guarantee convergence at a known rate. This approach provides a condition for trusting the

Manuscript received May 4, 2016; revised September 18, 2016; accepted October 10, 2016. Date of publication December 20, 2016; date of current version April 3, 2017. This paper was recommended for publication by Associate Editor H. Kress-Gazit and Editor T. Murphey upon evaluation of the reviewers' comments. This work was supported in part by a Task Order contract with the Air Force Research Laboratory, Munitions Directorate at Eglin AFB, in part by the U.S. National Geospatial Intelligence Agency under Grant HM0177-12-1-0006, and in part by the U.S. Department of Agriculture National Robotics Initiative under Grant 2013-67021-21074.

The authors are with the Department of Mechanical and Aerospace Engineering, University of Florida, Gainesville, FL 32611-6250 USA (e-mail: anuppari@ufl.edu; tenghu@ufl.edu; hychen@ufl.edu; wdixon@ufl.edu).

This paper has supplementary downloadable material available at <http://ieeexplore.ieee.org>.

Color versions of one or more of the figures in this paper are available online at <http://ieeexplore.ieee.org>

Digital Object Identifier 10.1109/TRO.2016.2627024

state estimates from the observer and an updated performance metric (via the error decay rate) based on the error growth rate during the periods when measurements are unavailable. These conditions could also be used to ease trajectory generation constraints. For example, traditional visual servoing requires that the features remain in the camera FOV, which may be difficult for a camera mounted on a nonholonomic vehicle. By relaxing the requirement that the target remain in the FOV, more efficient guidance laws may be designed.

Removing the continuous observation requirement has been studied for problems where the objective is to track the 2-D image coordinates of features that undergo temporary occlusions. For example, Sznaier *et al.* [15], [16] describe methods for learning a model of the feature motion, and using the model to predict feature motion when it is occluded. In contrast to using dynamic models, the results in [17]–[19] use visual context to increase the robustness of feature trackers to occlusions. All of these methods aid in tracking the feature location on the image plane (i.e., only the feature pixel coordinates are estimated), and must be used in conjunction with SfM techniques to provide a continuous estimate of the 3-D object coordinates in the presence of intermittent measurements, although there is still no guarantee that the SfM algorithms will be stable when provided intermittent measurements. In [20], an SfM technique that is robust to occlusions or feature tracking losses is developed, but only the shape of the object is recovered due to the orthogonal projection model, and not the 3-D position of the object relative to the camera. In contrast to such results, the object Euclidean coordinates are directly estimated in this paper, and sufficient conditions are provided to guarantee stability.

Many of the probabilistic approaches for SfM, or the broader visual simultaneous localization and mapping problem that solves the SfM problem during mapping, utilize a predictor similar to that developed in this paper or circumvent the intermittent sensing issue by only updating state estimates when new measurements are available (see [21] and [22] for an overview). However, these approaches are based on either linearizations of the nonlinear dynamics (e.g., [23]–[28]), and therefore only show local convergence, or are sample based (e.g., [29] and [30]), and therefore can only show optimal estimation in the limit as the number of samples approach infinity. Much of the recent literature on target tracking has focused on using suboptimal algorithms for tracking using simplified motion models (e.g., constant velocity, constant turn rate, etc.), with a focus on reduced complexity and improving practical performance, and do not analyze estimation error growth due to model uncertainty or show estimation error convergence [31], [32]. Some methods explicitly handle occlusions, though they either assume availability of range measurements that render the system linear, e.g., [33]–[35], or only estimate relative depth ordering and do not consider the range estimation problem, e.g., [36]. Conversely, the full nonlinear dynamics are analyzed in this paper, resulting in an arbitrarily large region of attraction around the zero estimation error trajectory, and the proposed observer–predictor structure has computing requirements that can be met by typical or low-end modern computers (e.g., see Section VII). Convergence and consistency proofs of probabilistic estimators typically require knowledge of the probability distribution

of the uncertainty in the system, and result in convergence in mean or in mean square. In comparison, analysis of deterministic observers typically assumes boundedness and some level of smoothness of disturbances, and yields asymptotic or exponential convergence. The primary contribution of this paper is in the development and analysis of a framework to show robustness to intermittent measurements when utilizing deterministic, image-based observers.

Filters that are robust to missing measurements have been developed for control and fault detection (cf. [37]–[53]). In results, such as [37], [40]–[44], [47]–[51], [53]–[64], measurement loss is modeled as a random Bernoulli process with known probability. As a result, filter stability can only be shown in the stochastic sense, i.e., the expected value of the estimation error is shown to asymptotically converge. In some cases (cf. [37], [43], [48], [50], [54]–[59], [64]), measurement loss is imperceptible, and measurements consisting of only noise are incorporated into the state estimates. In this paper, no assumption is made on the nature of switching; any switching sequence that meets an average dwell time condition and a total unstable activation time condition is shown to yield a stable estimate. For many machine vision applications, loss of feature tracking can be detected, and therefore we do not consider the case where erroneous measurements are incorporated into the state estimates.

This paper contrasts with our previous results given in [65], where it was shown that the simple approach of performing a zero-order hold (ZOH) on the state estimate when measurements are unavailable results in a stable estimator if dwell time conditions are satisfied. In [65], no motion model is used during the periods when measurements are not available, and therefore no estimate of the object position is produced during those periods. Moreover, only upper bounds on the object velocities are used to bound the growth of the error during the periods when measurements are unavailable, and therefore the position of the object is bounded by a sphere that grows with time at a rate proportional to the maximum object velocity. Consequently, the Lyapunov-like function grows with a bound based on the trigonometric tangent function, resulting in a stability condition on the maximum contiguous duration in which the object can remain hidden from the camera. In contrast, the stability conditions presented in this paper allow the object to remain hidden for arbitrarily large amounts of time, and object position estimates can be updated even when it is occluded, outside the camera FOV or between video frames. However, object velocities, or a motion model in the form of a feedback law, is required to achieve these results. Simulation results provide a comparison between the results in this paper and our result in [65]. The comparison demonstrates the tradeoff between the amount of information that is known about the target and the allowable flexibility in observation of the target for successful tracking. This work also adds value over our preliminary developments in [66]. Compared to [66], the performance of the developed method is also examined through simulations and experimental results. Moreover, this paper illustrates how a common observer design that only estimates partial states can be extended to full-state estimation and therefore can be used in the observer portion of the observer–predictor framework. Furthermore, comparison of the experimental results with the theoretically developed bounds as

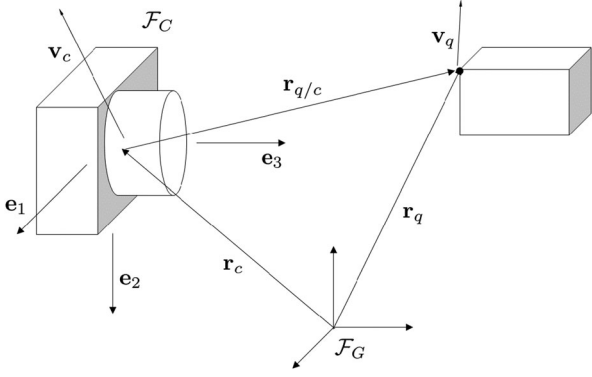


Fig. 1. Reference frames and coordinate systems of a moving camera observing a point on a moving target.

well as an implementation of the extended Kalman filter (EKF) are provided.

II. KINEMATIC MOTION MODEL

In the following development, Fig. 1 is used to develop the image kinematics, where \mathcal{F}_G denotes a fixed inertial reference frame with an arbitrarily selected origin and Euclidean coordinate system, and \mathcal{F}_C denotes a reference frame fixed to the camera. The right-handed coordinate system attached to \mathcal{F}_C has its origin at the principle point of the camera, $\mathbf{e}_3 \in \mathbb{R}^3$ axis pointing out and collinear with the optical axis of the camera, $\mathbf{e}_1 \in \mathbb{R}^3$ axis aligned with the horizontal axis of the camera, and $\mathbf{e}_2 \triangleq \mathbf{e}_3 \times \mathbf{e}_1 \in \mathbb{R}^3$. The vectors $\mathbf{r}_q \in \mathbb{R}^3$ and $\mathbf{r}_c \in \mathbb{R}^3$ represent the vectors from the origin of \mathcal{F}_G to a point on the object of interest and the camera principle point, respectively. The kinematics of the coordinates of the relative position vector expressed in the camera coordinate system, $\mathbf{r}_{q/c} \triangleq [X \ Y \ Z]^T \in \mathbb{R}^3$, are

$$\dot{\mathbf{r}}_{q/c} = \mathbf{v}_q - \mathbf{v}_c - \boldsymbol{\omega} \times \mathbf{r}_{q/c} \quad (1)$$

where $\mathbf{v}_q \triangleq [v_{q1} \ v_{q2} \ v_{q3}]^T \in \mathbb{R}^3$ is the inertial linear velocity of the point on the object¹ (henceforth denoted as the object velocity), $\mathbf{v}_c \triangleq [v_{c1} \ v_{c2} \ v_{c3}]^T \in \mathbb{R}^3$ is the inertial linear velocity of the camera, and $\boldsymbol{\omega} \triangleq [\omega_1 \ \omega_2 \ \omega_3]^T \in \mathbb{R}^3$ is the inertial angular velocity of the camera, all expressed in the camera coordinate system.

To facilitate the subsequent analysis, the states of the system are defined as $\mathbf{x} = [x_1, x_2, x_3]^T = [\frac{X}{Z}, \frac{Y}{Z}, \frac{1}{Z}]^T \in \mathbb{R}^3$. Taking the time derivative of the states, substituting in (1), and simplifying yields the perspective state dynamics of the form $\dot{\mathbf{x}} = g(t, \mathbf{x})$, where $g(t, \mathbf{x}) : [0, \infty) \times \mathbb{R}^3 \rightarrow \mathbb{R}^3$ is a function that nonlinearly depends on the partially measurable states, which can be expressed as

$$\begin{aligned} \dot{x}_1 &= \Omega_1 + \xi_1 + v_{q1}x_3 - x_1v_{q3}x_3, \\ \dot{x}_2 &= \Omega_2 + \xi_2 + v_{q2}x_3 - x_2v_{q3}x_3, \\ \dot{x}_3 &= v_{c3}x_3^2 - (\omega_2x_1 - \omega_1x_2)x_3 - v_{q3}x_3^2 \end{aligned} \quad (2)$$

¹This development can be extended to the case of multiple points on a single object to determine the six degree-of-freedom (DOF) position and orientation of the object rather than only the 3DOF position. In this case, the velocity of any point on the object can be determined from the linear and angular velocities of the object.

where $\Omega_1, \Omega_2, \xi_1, \xi_2 : [0, \infty) \times \mathbb{R}^3 \rightarrow \mathbb{R}$ are defined as

$$\begin{aligned} \Omega_1(t, \mathbf{x}) &= \omega_3x_2 - \omega_2 - \omega_2x_1^2 + \omega_1x_1x_2, \\ \Omega_2(t, \mathbf{x}) &= \omega_1 - \omega_3x_1 - \omega_2x_1x_2 + \omega_1x_2^2, \\ \xi_1(t, \mathbf{x}) &= (v_{c3}x_1 - v_{c1})x_3, \\ \xi_2(t, \mathbf{x}) &= (v_{c3}x_2 - v_{c2})x_3. \end{aligned} \quad (3)$$

See [67] for the explicit development of (2).

Assumption 1: The state \mathbf{x} is bounded, i.e., $\mathbf{x} \in \mathcal{X}$, where $\mathcal{X} \subset \mathbb{R}^3$ is a convex, compact set.

Remark 1: For the state estimates to converge to the states while remaining bounded, the states themselves must remain bounded. During periods in which the object is visible, bounds on the states are a result of the physical constraints on the imaging system. For image formation, the object must remain in front of the camera principle point by an arbitrarily small amount, $\epsilon \in \mathbb{R}$. This provides an arbitrarily small lower bound on Z and therefore an arbitrarily large upper bound on x_3 . Also, boundedness of the pixel coordinates of the object and boundedness of the camera intrinsic parameter matrix (see the imaging model in the next section) result in boundedness of x_1 and x_2 . During the periods in which measurements are unavailable, these physical constraints no longer apply. However, Assumption 1 requires that the object does not exhibit finite escape, even during the periods when the object is not visible to the camera. This restricts the relative motion of the object with respect to the camera; the object cannot move behind the camera, even during the periods when the object is not visible, else the state x_3 will pass through ∞ .

Assumption 2: The motion of the camera is measurable and bounded, in the sense that $v_{c1}, v_{c2}, v_{c3}, \omega_1, \omega_2$, and ω_3 are measurable and bounded.

Assumption 3: A motion model of the moving object is known and bounded, in the sense that either the object velocity, $\mathbf{v}_q \triangleq [v_{q1} \ v_{q2} \ v_{q3}]^T \in \mathbb{R}^3$, is known and bounded or the object velocities are given by $\mathbf{v}_q = \phi(\mathbf{x})$, where the known, continuous function $\phi : \mathbb{R}^3 \rightarrow \mathbb{R}^3$ is locally Lipschitz on \mathcal{X} .

An analytical expression for object velocities as a function of time is not required to generate the necessary signals v_{q1}, v_{q2} , and v_{q3} . For example, a feedback law in the form of

$$\dot{\mathbf{r}}_q = \phi_G(\mathbf{r}_q) \quad (4)$$

is sufficient to generate \mathbf{v}_q , where $\phi_G : \mathbb{R}^3 \rightarrow \mathbb{R}^3$ is Lipschitz and \mathbf{r}_q is expressed in the coordinate system attached to the inertial frame \mathcal{F}_G . However, in this case, the position and orientation of the camera is required to transform state estimates in the camera frame to position estimates in the ground frame. From (4), the signal \mathbf{v}_q is given by

$$\mathbf{v}_q = [\phi_1(x), \phi_2(x), \phi_3(x)]^T \triangleq R^T \phi_G(R\mathbf{r}_{q/c} + \mathbf{r}_c) \quad (5)$$

where $\phi_1, \phi_2, \phi_3 : \mathbb{R}^3 \rightarrow \mathbb{R}$, \mathbf{r}_c is expressed in the coordinate system attached to the inertial frame \mathcal{F}_G , $R \in SO(3)$ denotes the orientation of the camera in the sense that premultiplying by R rotates a vector expressed in the camera coordinate system to a vector expressed in the ground coordinate system, and $\mathbf{r}_{q/c}$ is

related to the states by

$$\mathbf{r}_{q/c} = \begin{bmatrix} \frac{x_1}{x_3} & \frac{x_2}{x_3} & \frac{1}{x_3} \end{bmatrix}^T.$$

Substituting (5) into (2) yields a new expression for $g(t, \mathbf{x})$ given by

$$\begin{aligned} \dot{x}_1 &= \Omega_1 + \xi_1 + \phi_1(x) x_3 - x_1 \phi_3(x) x_3, \\ \dot{x}_2 &= \Omega_2 + \xi_2 + \phi_2(x) x_3 - x_2 \phi_3(x) x_3, \\ \dot{x}_3 &= v_{c3} x_3^2 - (x_1 \omega_2 - x_2 \omega_1) x_3 - \phi_3(x) x_3^2. \end{aligned} \quad (6)$$

Although the object motion model, $\phi \triangleq [\phi_1(x), \phi_2(x), \phi_3(x)]^T$, is assumed to be known, the states are unknown and therefore the estimated object velocity, $\hat{v}_q \in \mathbb{R}^3$ is given by

$$\hat{v}_q = \phi(\hat{\mathbf{x}}).$$

A wide variety of object motions can be described by a feedback law in the form of (5). For example, consider the scenario of a vehicle moving with a known constant nominal speed. In this case, the velocity of the vehicle \hat{v}_q is determined based on the location of the vehicle (e.g., based on whether the vehicle is traveling on an East/West road or North/South road, and which side of the road the vehicle is on). The state estimates can also be used to determine if the vehicle is at an intersection, and \hat{v}_q can be adjusted based on that information. A model of the form in (4) can also be generated in cases where the object is undergoing projectile or orbital motion. In these cases, the object velocity is a function of the object position. Similarly, in eye-to-hand image-based visual servoing, a control law of the form in (4) is designed, and therefore known.

In applications where the object and camera are cooperative, the object can directly communicate its velocities to the camera. This is a common scenario in GPS-denied environments, where the object of interest might be a ground vehicle, which is being observed by a high altitude aerial vehicle with an active GPS signal [68], [69], or when multiple cooperative agents are each observing each other to reduce the overall position uncertainty growth rate [70]–[73]. Once the relative position vector is estimated, the geographic coordinates of the ground vehicle can be determined and continuously estimated even if the camera intermittently loses line of sight.

III. IMAGING MODEL

Using projective geometry, the image coordinates of the feature point, $\mathbf{p} = [u \ v \ 1]^T \in \mathbb{R}^3$, where $u, v \in \mathbb{R}$, are related to the normalized Euclidean coordinates, $\mathbf{m} \triangleq [\frac{X}{Z} \ \frac{Y}{Z} \ 1]^T \in \mathbb{R}^3$, by

$$\mathbf{p} = \mathbf{A}\mathbf{m}$$

where $\mathbf{A} \in \mathbb{R}^{3 \times 3}$ is the invertible camera intrinsic parameter matrix [74]. Since \mathbf{A} is invertible, the states x_1 and x_2 are measurable when the object is visible to the camera.

Remark 2: As explained in the remark proceeding Assumption 1, this planar projection model requires the object to remain in front of the camera. One method for circumventing this limitation is to recast the system in terms of spherical coordinates

(see [74, Chapter 3] or [75, Chapter 11]), which only has a singularity at the origin rather than the entire $Z = 0$ plane. This model would result in different dynamics than the system presented in (2). In an effort to broaden the applicability of the results presented in this paper, a planar projection model is considered to match the dynamics utilized in much of the observer literature (see Assumption 6).

Assumption 4: The camera intrinsic parameter matrix \mathbf{A} is known.

Remark 3: The intrinsic parameters can be determined through a calibration procedure [74].

Assumption 5: The object is uniquely identifiable from image projections.

Remark 4: Algorithms such as the Kanade–Lucas–Tomasi [76] feature tracker have been developed to track image features in consecutive frames of a video stream, however these may not be sufficient for object tracking if the object temporarily leaves the FOV or becomes occluded; these feature trackers typically do not differentiate between new features and features that have been tracked previously and therefore cannot track an object continuously through intermittent measurements, where continuity or small deviation assumptions may not hold. Other feature descriptors, such as SIFT [77] and SURF [78], have been used to match objects across affine transformations, and therefore may be more robust to temporary loss of sight. Recently, machine learning techniques have been used to recognize and localize objects in images [79], [80]. A combination of these techniques can be used to track a feature through multiple periods of intermittent visibility. See [81] and [82] for a survey on feature trackers and [79] for examples and performance of modern object localization algorithms.

IV. STRUCTURE ESTIMATION OBJECTIVE

To quantify the structure estimation objective, let the state estimation error $\mathbf{e} \in \mathbb{R}^3$ be defined as

$$\mathbf{e} = \mathbf{x} - \hat{\mathbf{x}} \quad (7)$$

where $\hat{\mathbf{x}} \in \mathbb{R}^3$ denotes the continuous state estimate. Consider the family of systems

$$\dot{\mathbf{e}} = f_p(t, \mathbf{x}, \hat{\mathbf{x}}) \quad (8)$$

where $f_p : [0, \infty) \times \mathbb{R}^3 \times \mathbb{R}^3 \rightarrow \mathbb{R}^3$, $p \in \{s, u\}$, s is an index referring to the system when measurements are available, and u is an index referring to the system when measurements are unavailable. When the object is in view, the states x_1 and x_2 are measurable, and the error dynamics are given by

$$f_s = g(t, \mathbf{x}) - \dot{\hat{\mathbf{x}}} \quad (9)$$

where the state estimate dynamics $\dot{\hat{\mathbf{x}}}$ are governed by an observer and $g(t, \mathbf{x})$ was introduced prior to (2). When the object is outside the camera FOV, the state estimates are updated using the object motion model described in Assumption 3 and a predictor of the form

$$\dot{\hat{\mathbf{x}}} = \text{proj}(g(t, \hat{\mathbf{x}})) \quad (10)$$

resulting in the error dynamics

$$f_u = g(t, \mathbf{x}) - \text{proj}(g(t, \hat{\mathbf{x}})) \quad (11)$$

where $\text{proj}(\cdot)$ is a smooth projection operator (see [83, Appendix E], [84, Remark 3.7]) with bounds based on the state bounds of Assumption 1 and the velocity bounds in Assumptions 2 and 3. Since $g(t, \mathbf{x})$ is continuously differentiable with respect to \mathbf{x} on the compact set \mathcal{X} , the mean value theorem can be invoked to bound the error dynamics during the periods when measurements are unavailable as

$$\|f_u\| \leq K \|e\| \quad (12)$$

where $K \in \mathbb{R}$ is a bounded constant.

Assumption 6: An observer for the state \mathbf{x} is used so that when the states x_1 and x_2 are measurable, the state estimation error is globally exponentially convergent at a rate of $\lambda_{\text{on}} \in \mathbb{R}_{>0}$, i.e., $\|e(t)\| \leq C \|e(t_0)\| \exp[-\lambda_{\text{on}}(t - t_0)]$ for any initial condition $e(t_0)$, with $t_0 \in \mathbb{R}_{\geq 0}$ and some positive constant $C \in \mathbb{R}$.

Remark 5: Exponentially convergent observers for image-based structure estimation that satisfy Assumption 6 are available from results such as [6], [9], [10], [85]–[87]. Many of these results utilize a persistence of excitation condition as well as gain conditions to yield exponential convergence. Any conditions required by the observer are also inherited here. Also, in some cases (e.g., [6]), only the unmeasurable state, $x_3(t)$, is estimated. In these cases, the observer can be augmented as exemplified in the Appendix to maintain continuity of the state estimates as is required in the following stability analysis (i.e., to guarantee the system is a switched system as opposed to a hybrid system with discontinuous states). Although directly using the states x_1 and x_2 when they are measurable may yield faster estimation (in the sense that the first two elements of e would be identically zero whenever measurements are available), the gains in the augmentation can be made arbitrarily large to yield an arbitrarily close approximation to direct use of the states x_1 and x_2 without violating continuity assumptions.

V. STABILITY ANALYSIS

To facilitate the following development, let $T^u(t, \tau)$ denote the total time the subsystem u is active in the time interval $[\tau, t]$, where $0 \leq \tau \leq t$. Also, let $N_\sigma(t, \tau) \in \mathbb{N}$ denote the number of switches of the switching signal $\sigma : [0, \infty) \rightarrow \{s, u\}$ during the time interval (τ, t) . Then, using the definition from [88], the switching signal σ is said to have an average dwell time τ_a if there exists constants $N_0, \tau_a \in \mathbb{R}_{>0}$ such that

$$N_\sigma(t, \tau) \leq N_0 + \frac{t - \tau}{\tau_a}, \quad \forall t \geq \tau \geq 0.$$

Finally, let \mathcal{P} be an index set with partition $\{\mathcal{P}_s, \mathcal{P}_u\}$ for the family of systems

$$\dot{\eta} = \phi_p(\eta, t), \quad \forall p \in \mathcal{P} \quad (13)$$

where $\eta \in \mathbb{R}^n$, $t \in [0, \infty)$, and $\phi_p : \mathbb{R}^n \rightarrow \mathbb{R}^n$.

Based on Assumption 6, the state estimate errors will converge to zero when measurements are available. Similarly, when measurements are unavailable, the growth of the estimation errors are bounded by an exponential based on (8) and (12). Hence, a quadratic Lyapunov-like function is expected to evolve similar to Fig. 2 across multiple instances of losing and regaining measurement availability. The goal is to show that, despite intermittent growth in the Lyapunov-like function, the overall trend

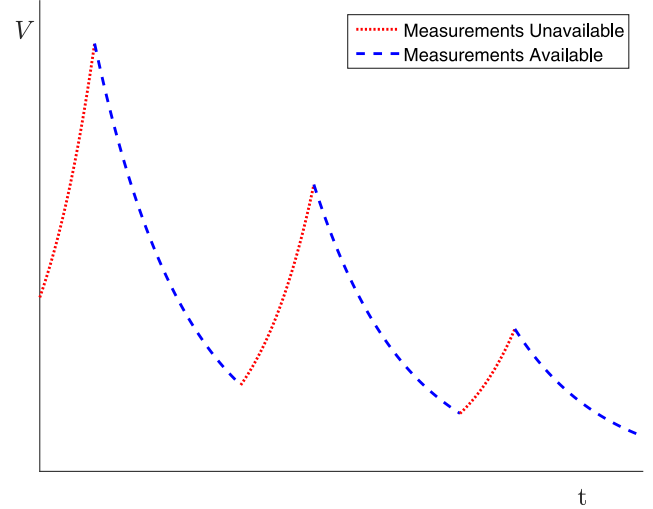


Fig. 2. Evolution of a Lyapunov-like function across multiple periods of losing and regaining visibility of the object.

is convergence to zero, and therefore convergence of the estimation errors. Lemma 1 shows that for a set of exponentially stable and exponentially unstable Lyapunov-like functions, the overall trend is convergence to zero if more time is spent in stable systems (proportional to the decay and growth rates of the stable and unstable systems, respectively) and if switching between systems does not occur too often, on average. Using this result, Theorem 1 indicates that the vision-based estimation approach developed in this paper is exponentially stable by developing Lyapunov-like functions that satisfy the hypotheses of Lemma 1.

Lemma 1: Consider the family of systems in (13). Suppose there exists continuously differentiable functions $V_p : \mathbb{R}^n \times [0, \infty) \rightarrow \mathbb{R}$, strictly positive constants $c_1, c_2, \lambda_s, \lambda_u \in \mathbb{R}_{>0}$, and constant $\mu \in \mathbb{R}$ greater than 1, such that

$$c_1 \|\eta\|^2 \leq V_p(\eta, t) \leq c_2 \|\eta\|^2$$

$$\frac{\partial V_p}{\partial t} + \frac{\partial V_p}{\partial \eta} \phi_p(\eta, t) \leq -\lambda_s V_p(\eta, t), \quad \forall p \in \mathcal{P}_s$$

$$\frac{\partial V_p}{\partial t} + \frac{\partial V_p}{\partial \eta} \phi_p(\eta, t) \leq \lambda_u V_p(\eta, t), \quad \forall p \in \mathcal{P}_u$$

$$V_p \leq \mu V_q, \quad \forall p, q \in \mathcal{P}.$$

If there exists positive constants $\rho, T_0 \in \mathbb{R}_{\geq 0}$, such that

$$\rho < \frac{\lambda_s}{\lambda_s + \lambda_u}$$

$$T^u(t, \tau) \leq T_0 + \rho(t - \tau), \quad \forall t \geq \tau \geq 0$$

and if $\sigma : [0, \infty) \rightarrow \mathcal{P}$ is a piecewise constant, right continuous switching signal with average dwell time

$$\tau_a > \frac{\ln \mu}{\lambda_s(1 - \rho) - \lambda_u \rho}$$

then the switched system

$$\dot{\eta} = \phi_\sigma(\eta, t)$$

is globally exponentially stable.

Proof: Lemma 1 is an extension to Theorem 2 in [89] for nonautonomous systems with nonautonomous functions V_p . The majority of the proof is omitted since it is identical to the proof of Lemma 1 in [89]. However, in this case, the functions $\alpha_1, \alpha_2 \in \mathcal{K}_\infty$ are quadratic and the trajectory of the switched system can be reduced to

$$\|\eta\| \leq \left[\frac{c_2}{c_1} \mu^{N_0} \exp((\lambda_s + \lambda_u) T_0) \right] \|\eta(0)\| \exp(-\lambda(t - t_0))$$

where $\lambda \triangleq \frac{1}{2}(\lambda_s - (\lambda_s + \lambda_u)\rho - \frac{\ln \mu}{\tau_a}) \in (0, (1 - \rho)\lambda_s + \rho\lambda_u) \subset \mathbb{R}_{>0}$. ■

Theorem 1: The switched system

$$\dot{\mathbf{x}} = f_\sigma(t, \mathbf{x}, \hat{\mathbf{x}})$$

generated by the family of systems described by (8)–(11) and piecewise constant, right continuous switching signal $\sigma : [0, \infty) \rightarrow \{s, u\}$ is globally exponentially stable provided that the switching signal σ satisfies the total unstable activation time condition

$$T^u(t, \tau) \leq T_0 + \rho(t - \tau), \quad \forall t \geq \tau \geq 0 \quad (14)$$

and average dwell time condition

$$\tau_a > \frac{\ln \mu}{\lambda_s(1 - \rho) - \lambda_u \rho}, \quad (15)$$

where $T_0 \in \mathbb{R}$ is an arbitrary positive constant and $\rho, \lambda_s, \lambda_u, \mu \in \mathbb{R}$ are known positive constants that satisfy $\mu \geq 1$ and $\rho < \frac{\lambda_s}{\lambda_s + \lambda_u}$.

Proof: Via converse Lyapunov theorems [90, Theorem 4.14], the existence of an exponential state tracking observer from Assumption 6 implies the existence of a Lyapunov function $V_s : [0, \infty) \times \mathbb{R}^3 \rightarrow \mathbb{R}$ that is norm bounded (i.e., $c_1 \|\mathbf{e}\|^2 \leq V_s(t, \mathbf{e}) \leq c_2 \|\mathbf{e}\|^2$ for some $c_1, c_2 \in \mathbb{R}_{>0}$) and exponentially decaying (i.e., $\dot{V}_s \leq -\lambda_s V_s$ for some $\lambda_s \in \mathbb{R}_{>0}$), during the periods in which measurements are available. Consider a continuously differentiable, Lyapunov-like function defined as $V_u(\mathbf{e}) \triangleq c_5 \|\mathbf{e}\|^2$, where $c_5 \in \mathbb{R}$ is bounded by $c_1 \leq c_5 \leq c_2$. Using (12), the growth of V_u during the periods in which the object is outside the camera FOV can be bounded as

$$\dot{V}_u \leq 2c_5 K \|\mathbf{e}\|^2 \leq \lambda_u V_u,$$

where $\lambda_u \triangleq 2K$. From the definition of V_u and the norm bounds on V_s

$$V_p \leq \mu V_q, \quad \forall p, q \in \{s, u\}, \quad (16)$$

where $\mu \triangleq \frac{c_2}{c_1}$. Using Lemma 1, the system is globally exponentially stable for any switching signal that satisfies (14) and (15) with trajectory

$$\|\mathbf{e}\| \leq \|\mathbf{e}(t_0)\| C \exp(-\lambda(t - t_0)),$$

decay rate $\lambda \triangleq \frac{1}{2}(\lambda_s - (\lambda_s + \lambda_u)\rho - \frac{\ln \mu}{\tau_a}) \in (0, (1 - \rho)\lambda_s + \rho\lambda_u) \subset \mathbb{R}_{>0}$ and positive constant $C \triangleq \frac{c_2}{c_1} \mu^{N_0} \exp((\lambda_s + \lambda_u)T_0) \in \mathbb{R}_{>0}$. ■

Remark 6: In application, the constraint on the unstable activation time (i.e., (14)) is trivially satisfied. An arbitrarily large amount of time can be spent in the unstable system (i.e., measurements are unavailable), and T_0 can be increased to compensate. This condition is only relevant in the limit as $t \rightarrow \infty$,

where, on average, more time needs to be spent in the stable system (i.e., measurements are available) based on the relative convergence and divergence rates of the two systems. However, by increasing T_0 to satisfy stability conditions for large unstable activation times $T^u(t, \tau)$, the bounding envelope on the estimation error increases exponentially. This highlights the importance of increasing the duration in which the object is visible, even in the short term.

Remark 7: The average dwell time, τ_a , and the total allowable invisibility time in (14), are functions of the error decay and growth rates of the observer and predictor. As the observer convergence rate increases or the predictor divergence rate decreases, the upper bound on the allowable ρ increases, increasing the total allowable time duration in which the object can remain outside of the camera FOV. In addition, increasing ρ decreases the lower bound on the allowable average dwell time, enabling the use of a larger set of switching signals. However, increasing ρ decreases the convergence rate of the switched system; by allowing longer durations in which measurements are unavailable (from (14)), the error of the switched system is slower to converge. Conversely, as $\rho \rightarrow 0$, the allowable amount of time without measurements decreases and the convergence rate of the switched system increases. The limiting case where $\rho = 0$ denotes the case when measurements are available for all time after a finite number of switches. Finally, switching signals with larger average dwell times also increase the switched system convergence rate since the jumps in the Lyapunov-like functions occur less frequently.

Remark 8: The average dwell time conditions in Lemma 1 and Theorem 1 come as a result of the possibility that the Lyapunov-like functions for each subsystem may differ, even though they all satisfy a common quadratic bound. However, in some cases (e.g., [6], [10]), the constants c_1 and c_2 are equal, and c_5 can be chosen as $c_5 = c_1 = c_2$. Therefore, $\mu = 1$ and the average dwell time condition reduces to the trivial condition $\tau_a > 0$.

VI. SIMULATION

Simulations were performed using MATLAB to verify the robustness to measurement loss of the proposed observer and predictor estimation scheme. The observer in [85] was used to satisfy Assumption 6 and estimate the states when measurements were available, while the predictor in (10) was used when measurements were unavailable. Camera and object velocities, $\mathbf{v}_c(t) = [2 \ 1 \ 0.5 \cos(t/2)]^T$ m/s, $\boldsymbol{\omega}(t) = [0 \ 0 \ 1]^T$ rad/s, and $\mathbf{v}_q(t) = [0.5 \ 0 \ 0]^T$ m/s and observer matrices

$$A = \begin{bmatrix} 0 & -1 & 2 \\ 1 & 0 & 1 \\ 0 & 0 & 0 \end{bmatrix}, \quad C = \begin{bmatrix} 1 & 0 & 0 \\ 0 & 1 & 0 \end{bmatrix}, \quad D = \begin{bmatrix} 1 \\ 0 \\ 0 \end{bmatrix},$$

$$K = \begin{bmatrix} 0.8278 & 0 \\ 0 & 0.8278 \\ -1.5374 & 0 \end{bmatrix}, \quad Y = \begin{bmatrix} 0 & 0 \\ 0 & -1 \\ 0 & -1.5374 \end{bmatrix}$$

were set to match the simulation parameters in [85]. The switching signal σ was generated with randomly selected dwell times.

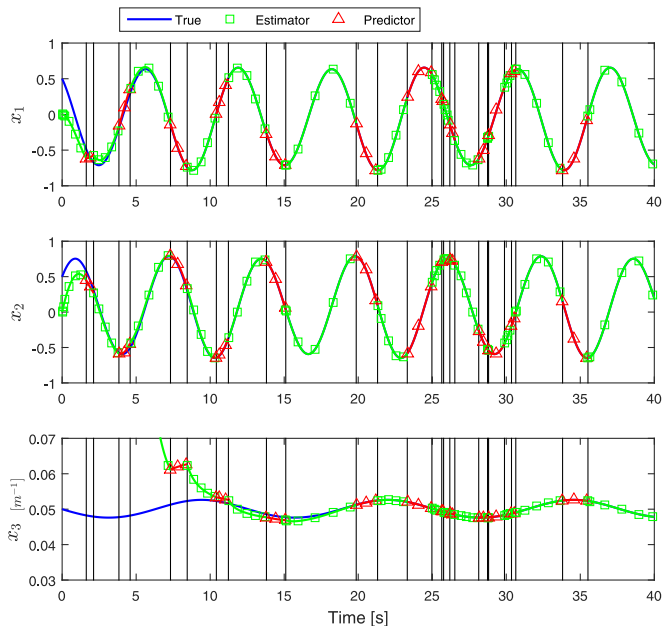


Fig. 3. True and estimated states, utilizing a predictor to evolve the state estimates when measurements are unavailable. Vertical lines represent switching times, e.g., the first vertical line represents the time when the object is no longer visible, and the predictor is started with the last state estimate from the estimator, the second vertical line represents the time when the object is in view again and the estimator is restarted with the state estimate from the predictor, etc.

The dwell times were selected from a uniform random distribution between 0 and 5 s, and 0 and 2 s for the s and u subsystems, respectively. Simulation results are shown in Fig. 3 with the switching times shown as vertical lines where the first vertical line represents the time when the object is no longer visible (i.e., the predictor is started with the last state estimate from the estimator), and the next vertical line represents the time when the object is in view again and the estimator is restarted with the state estimate from the predictor, etc.

The exponential trajectories for both subsystems developed in the analysis are reflected in the simulation results. For example, the divergence of the predictor lessens as $\hat{\mathbf{x}}$ approaches \mathbf{x} . This is expected, since exponential solutions are dependent on the initial condition, and as the estimator converges, the initial error at every predictor activation approaches zero.

An ad hoc approach for state estimation while undergoing intermittent measurements would be to implement a ZOH during periods in which measurements are unavailable. A simulation using ZOH was also performed, where $\hat{\mathbf{x}}$ was defined by the observer in [85] during the periods when measurements were available, and state estimates were not updated (i.e., $\dot{\hat{\mathbf{x}}} = 0$) during the periods in which measurements were unavailable, with the last estimate being used to reinitialize the observer when measurements became available. As shown in Fig. 4, using the same switching signal as in the previous simulation, the performance greatly degrades, with no indication of convergence. Comparing the results from Figs. 3 and 4 indicate that the predictor not only provides accurate state estimates when measurements are unavailable, but also aids in observer convergence when measurements are available by reinitializing the

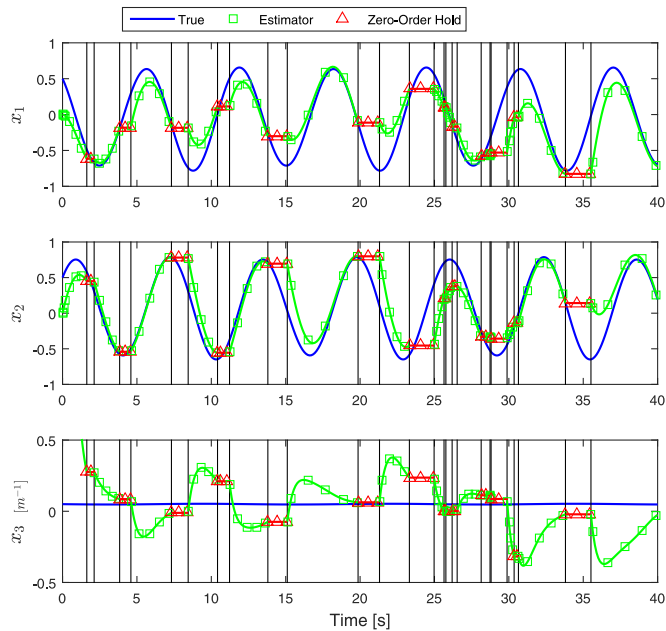


Fig. 4. True and estimated states without a predictor. State estimates are held constant until measurements are available. Vertical lines represent switching times.

observer with a more accurate initial state estimate. On the other hand, using a ZOH, the initial error at every time at which the observer is activated is larger (since the error grows at a tangential rate [65] instead of an exponential rate), and therefore the estimator requires more time to converge. This demonstrates the tradeoff mentioned in the introduction; by utilizing more information (i.e., velocity information of the object when not in view), a predictor can be utilized to relax dwell time conditions and ensure estimator convergence in the presence of a wider class of switching signals. However, if velocity information is not available, the more stringent conditions described in [65] must be satisfied to ensure convergence.

VII. EXPERIMENTS

Experiments were also performed to verify the theoretical results. The overall goal of the experiment was to represent the scenario of tracking the Euclidean position of a cooperative mobile vehicle in a GPS-denied environment via a camera. Specifically, the objective was to demonstrate the convergence of the relative position estimation errors when the estimator and predictor structure described in Section IV is implemented. An IDS UI-1580SE camera with 2-pixel binning enabled and a lens with a 90° FOV was used to capture 1280×960 pixel resolution images at a rate of approximately 15 frames per second. A Clearpath Robotics TurtleBot 2 with a Kobuki base was utilized as a GPS-denied mobile vehicle simulant. An augmented version of the observer in [6] provided range estimates while the mobile robot was visible (details are given in the Appendix). A fiducial marker with a corresponding tracking software library (see [91] and [92]) was used to repeatably track the image feature pixel coordinates and 3-D orientation of the mobile robot while it was in view. Although the library is capable of utilizing

marker scale information to reconstruct the fully scaled relative Euclidean position between the camera and the marker, the scale information was not necessary for implementation, and was not used in the experiment. The optic flow signals (i.e., derivatives of the measurable states) required for the observer were approximated via finite difference.

A NaturalPoint, Inc. OptiTrack motion capture system was used to record the ground truth pose of the camera and target at a rate of 360 Hz. The pose provided by the motion capture system was also used to estimate the linear and angular velocities of the camera necessary for the range observer, where the current camera velocity estimates were taken to be the slope of the linear regression of the 20 most recent pose data points. The wheel encoders and gyroscope onboard the mobile robot provided estimates of the linear and angular velocity of the mobile robot, expressed in the robot body coordinate system, which were communicated to the range observer. When the robot was in the camera FOV, the fiducial marker tracking algorithm orientation estimate was used to rotate the linear and angular velocities of the robot into the camera frame. When the robot was outside the camera FOV, the relative orientation between the camera and robot was estimated via dead-reckoning with the onboard gyroscope.

Two experiments were performed. In the first experiment, the camera was mounted on a stationary tripod, while the mobile robot was driven via remote control in an arbitrary motion, including leaving and entering the camera FOV. In the second experiment, the camera was moved by hand in an arbitrary motion, while the TurtleBot was sent constant forward velocity and angular turn rate commands, resulting in an approximately circular path. In this experiment, the intermittent measurements were caused by both the TurtleBot leaving the camera FOV, and an object placed directly in front of the camera lens, completely occluding the scene. The supplementary video accompanying this paper gives a representative sample of the motion of the mobile robot and the camera during both these experiments, and is available for download at <http://ieeexplore.ieee.org>. The resulting evolution of the state estimates and the reconstructed Euclidean coordinates of the target are shown in Figs. 5 and 6 for the first experiment, and Figs. 8 and 9 for the second experiment. In both cases, the estimates track the true values despite the intermittent visibility of the mobile robot.

Comparing the two experiments, the predictor appears to perform better in the case of a static camera. This reflects the prediction error growth rate bounds developed in the theoretical analysis; the growth rate is based on the camera and target velocity, and therefore is larger when both are moving. The estimator also appears to perform better in the case of a static camera. This is due to camera rotation about the X - or Y -axes resulting in large changes in x ; the pixel coordinates of a distant object move slowly when the camera is purely translating, but move quickly when the camera rotates. Therefore, any error or delay in the angular velocity signal has a much larger effect on performance, and in the moving camera experiment, the numerical method used to estimate the camera angular velocity results in more error (due to suppression of high-frequency components) and delay (due to using “old” data) compared to the static

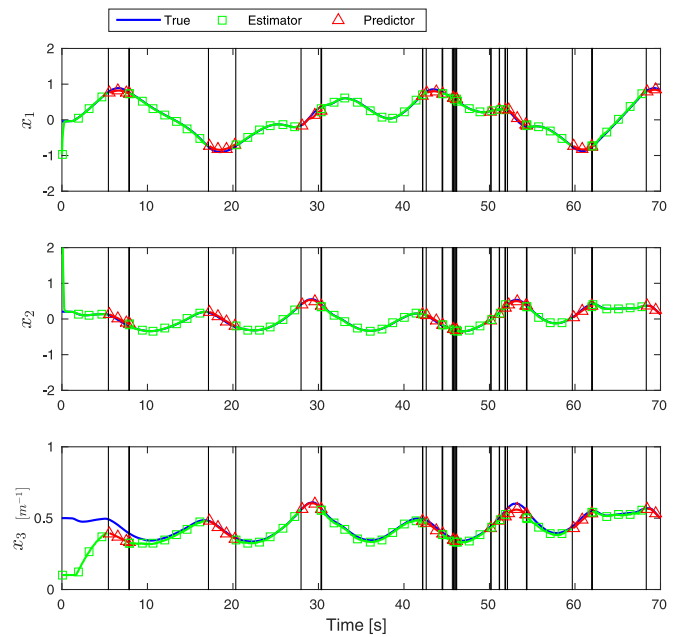


Fig. 5. State estimates from the experiment with a static camera. Vertical black lines denote switches.

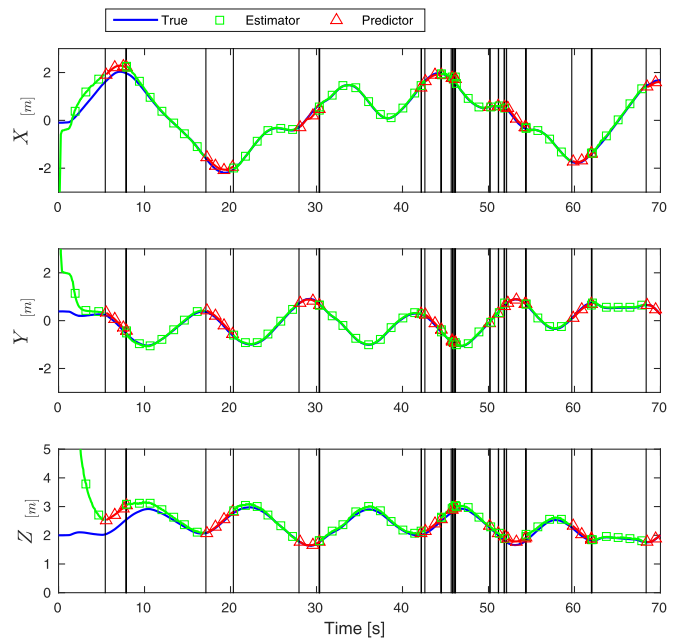


Fig. 6. Reconstructed Euclidean coordinates of the target from the experiment with a static camera. Vertical black lines denote switches.

camera case, where the angular velocity estimate error is purely noise.

As can be seen in Figs. 7 and 10, during periods when the object is not visible, the estimation error grows since there is no feedback from image measurements. However, exponential error growth would manifest as lines with constant positive slope on the log scale plots, whereas in the results, the errors increase and then decrease, indicating that the estimation error

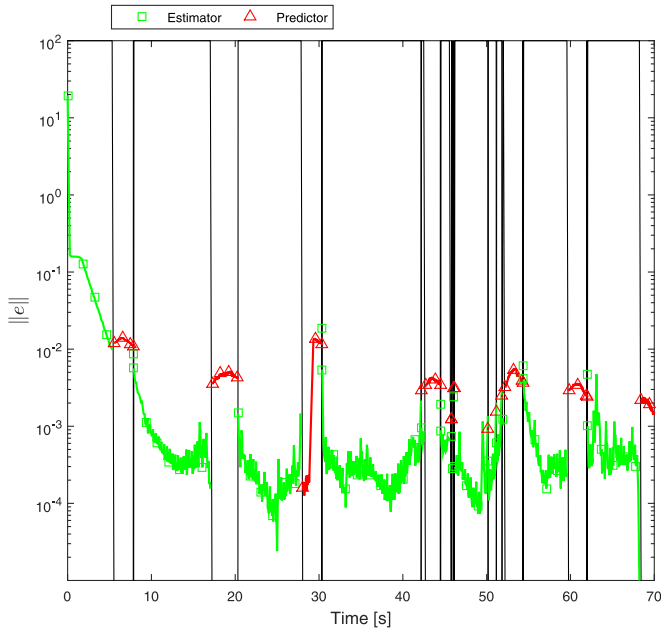


Fig. 7. State estimation errors from the experiment with a static camera. Vertical black lines denote switches.

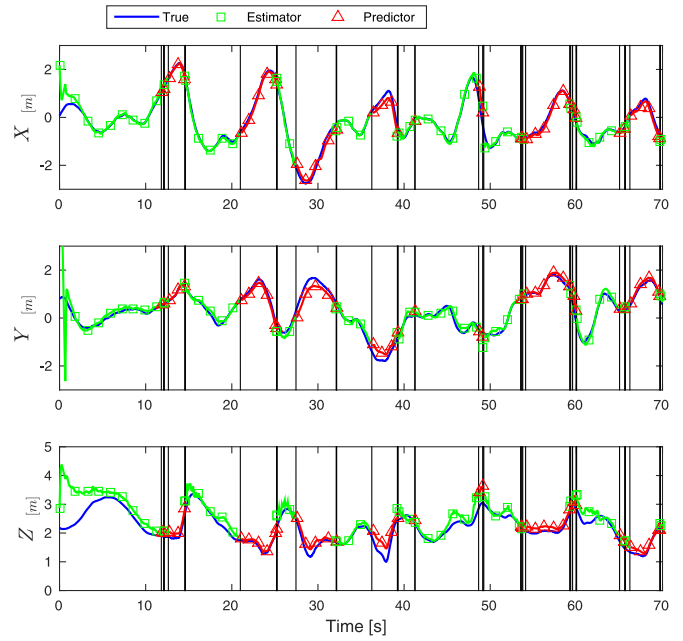


Fig. 9. Reconstructed Euclidean coordinates of the target from the experiment with a moving camera. Vertical black lines denote switches.

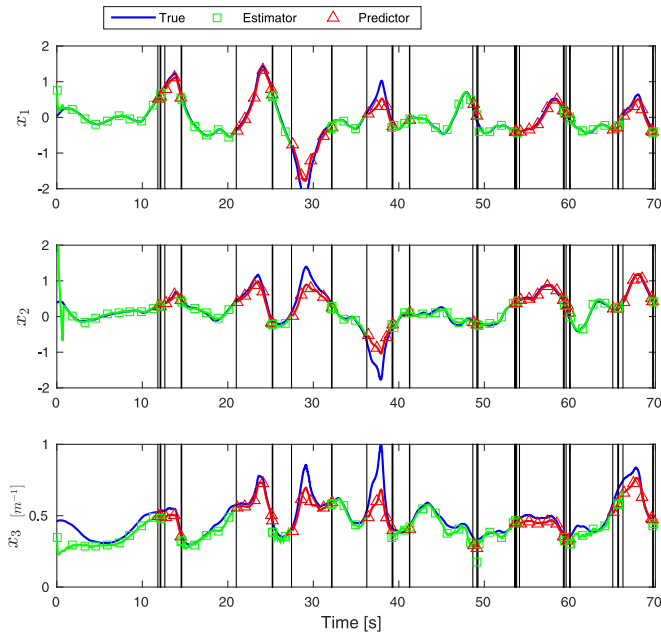


Fig. 8. State estimates from the experiment with a moving camera. Vertical black lines denote switches.

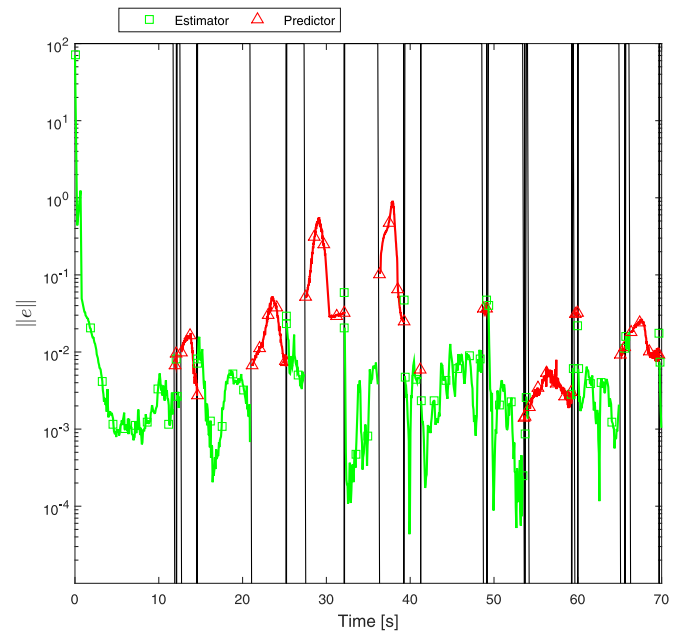


Fig. 10. State estimation errors from the experiment with a moving camera. Vertical black lines denote switches.

growth bounds used in the stability analysis in Section V are conservative.

To analyze the growth of the estimation error during periods when measurements are unavailable, the mean value theorem was used to develop a linear bound on f_u , as shown in (12). However, based on the quadratic terms in (2), the bounding constant K may need to be extremely large to bound f_u throughout the bounded set \mathcal{X} . Since only bounds on the states and velocities are available, the calculated value of K may also

be larger than the smallest constant that bounds f_u during a specific application. To investigate the conservativeness of K , and therefore the conservativeness of the exponential bound developed in Theorem 1, Figs. 11 and 12 show the error and its corresponding time derivative during each experiment, as well as the linear best fit line, minimum bounding line, and bounding line calculated based on the known quantities in Assumptions 1 and 2. For the experiment with a static camera, the best fit line (blue) had a slope of 0.1862, the minimum bound (green)

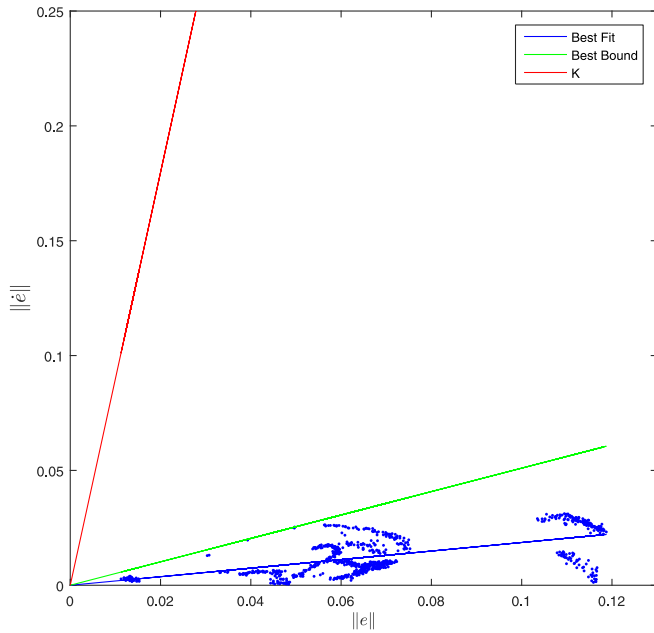


Fig. 11. Error growth magnitude as a function of the magnitude of the error, and corresponding bounds, for the experiment with a static camera.

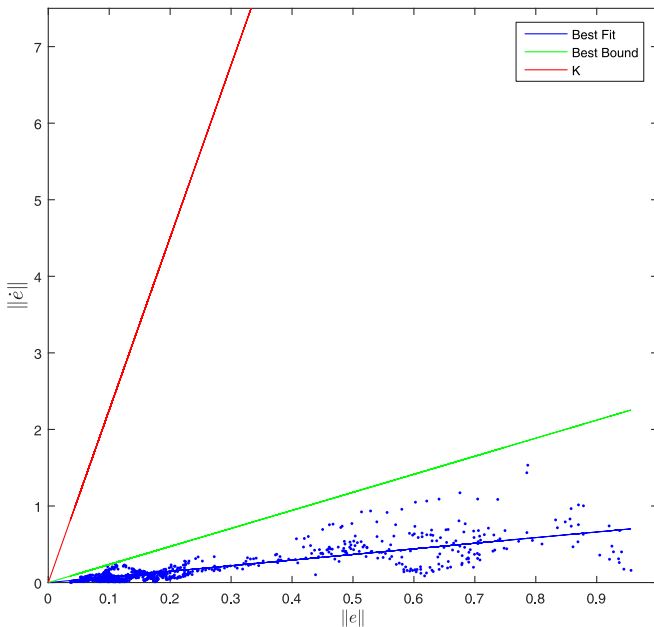


Fig. 12. Error growth magnitude as a function of the magnitude of the error, and corresponding bounds, for the experiment with a moving camera.

had a slope of 0.5098, and the calculated K (red) was 8.987. For the experiment with the moving camera, these values were 0.7337, 2.357, and 22.54, respectively. In both cases, the calculated bounds were an order of magnitude greater than the ideal bound; however, this is expected due to the conservative nature of Lyapunov analysis.

An additional experiment was performed using a motion model of the target (as described in Assumption 3 and the preceding explanation) rather than directly communicated velocities. In this experiment, the camera was kept stationary, and

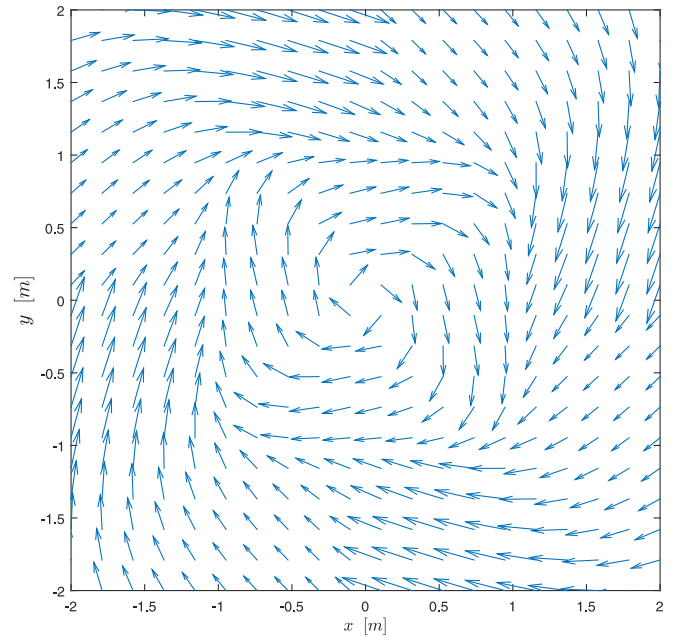


Fig. 13. During one experiment, the target was commanded to follow this vector field.

a velocity field of the form shown in Fig. 13 was prescribed in the world coordinate system, and a low-level controller was implemented to have the mobile robot follow the velocity field, though it should be noted that the robot did not follow the velocity field exactly due to the nonholonomic constraints of the robot and limits on the wheel velocity. The velocity field was rotated into the camera coordinate system and used as a velocity estimate of the robot in the predictor. For simplicity, camera feedback was artificially blocked at set intervals. The results of this experiment are shown in Figs. 14–16. Despite the actual target velocities being unknown, the state estimates generated by the observer/predictor framework successfully track the true states, with steady-state performance similar to that of the first two experiments, as shown in Fig. 16, and as compared to Figs. 7 and 10.

In the error plots of the preceding experiments (Figs. 7, 10, and 16), the estimation error appears to discretely change during switches. This is due to how feature tracking loss was detected: if new feature tracking data are not available for 0.2 s, the predictor is activated. This delay causes a slight discontinuity in the estimation error, which is exacerbated by the log scale on the error plots. The discontinuities seem largest when the estimates are within the noise floor of the system, i.e., in Fig. 16, compare the first set of switches during 0–10 s to the remaining switches. This also explains why the predictor appears to outperform the estimator in rare instances; if the target, by chance, happens to move toward the estimate during this delay period, the predictor will be initialized with a better estimate, and the exponential bound developed in the analysis, combined with the faster loop times due to only needing velocity information which was available at 360 Hz, dictates better prediction.

Finally, an EKF was implemented as an example of a typical probabilistic approach, where the robustness to intermittent

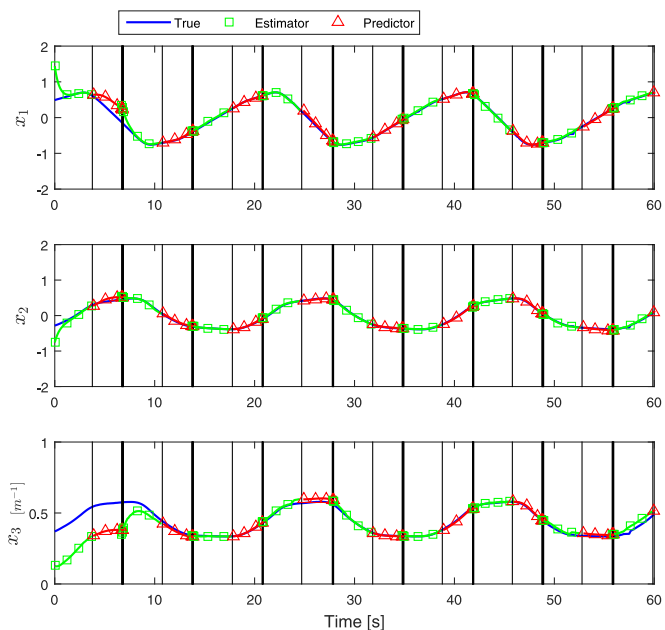


Fig. 14. State estimates from the experiment where the target followed a known vector field. Vertical black lines denote switches.

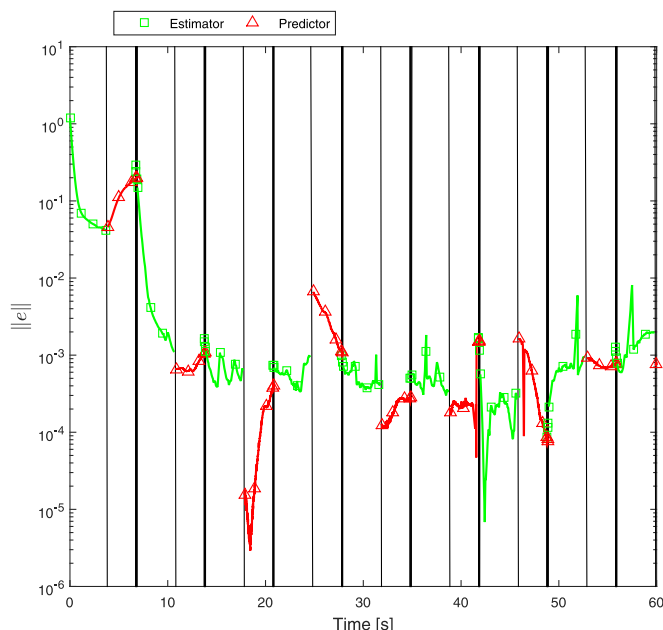


Fig. 16. State estimation errors from the experiment where the target followed a known vector field. Vertical black lines denote switches.

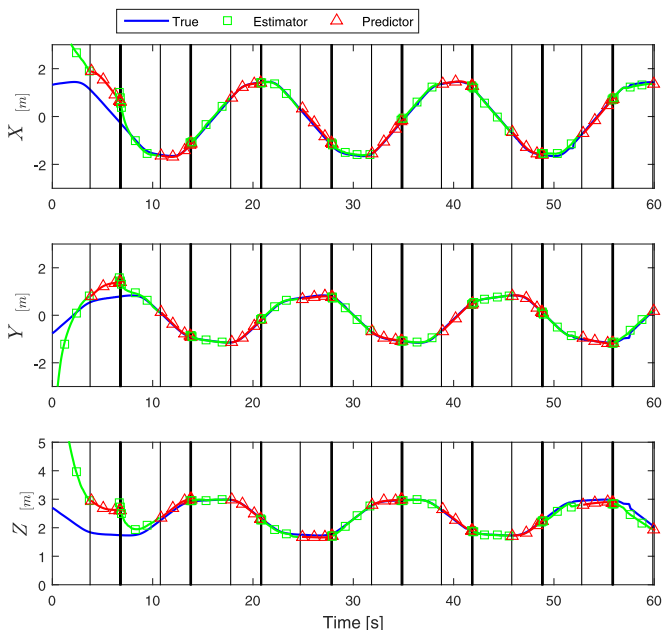


Fig. 15. Reconstructed Euclidean coordinates of the target from the experiment where the target followed a known vector field. Vertical black lines denote switches.

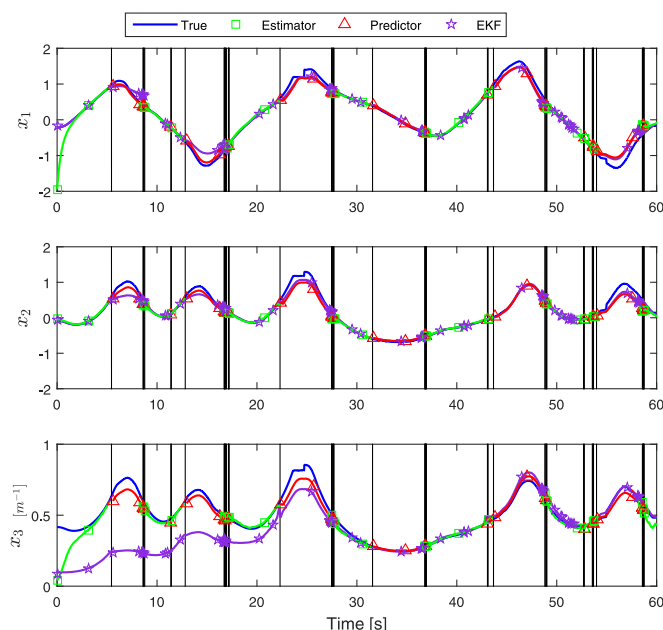


Fig. 17. State estimates from the experiment where the target followed a known vector field. Vertical black lines denote switches.

measurements is inherent to the predictor–corrector structure of these types of approaches. For this implementation, the covariance matrices were set based on an estimated 1 pixel uncertainty in the measurements, and 0.1 m/s uncertainty in the velocity information used in the dynamic model. These values were selected based on the uncertainty of the feature tracking as well as the uncertainty in the inputs to the process (the dynamic model is a purely kinematic model with no uncertain parameters, hence, the only uncertainty in the process comes

from the uncertain inputs, i.e., the measured velocities, which were estimated as described previously). The results of this experiment are shown in Figs. 17–19, where it is apparent that convergence of the state estimate generated by the EKF is much slower compared to the nonlinear observer implemented in the first two experiments. However, in many applications, the covariance matrices are used as tuning parameters, i.e., treated as gains, rather than selected based on the actual uncertainty in the system, and therefore estimation convergence performance may

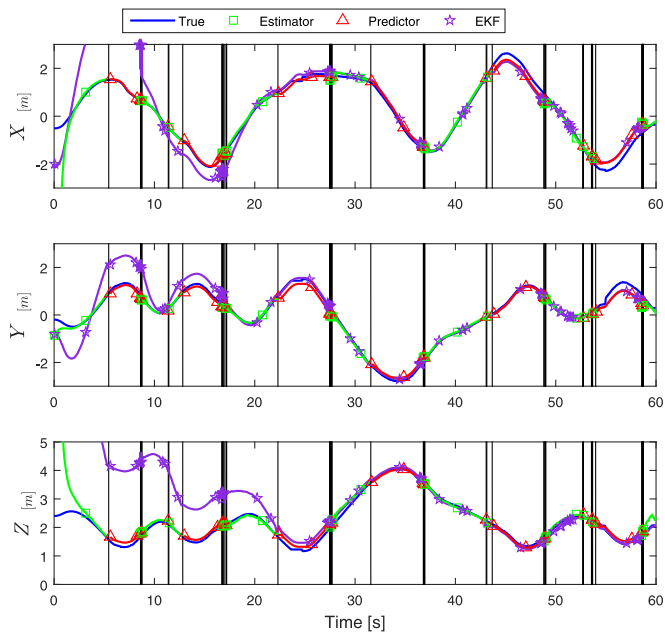


Fig. 18. Reconstructed Euclidean coordinates of the target from the experiment where the target followed a known vector field. Vertical black lines denote switches.

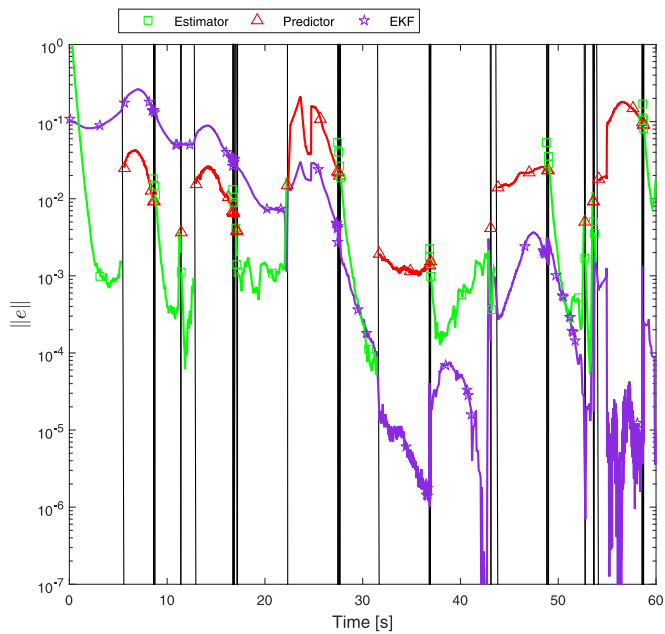


Fig. 19. State estimation errors from the experiment the target followed a known vector field. Vertical black lines denote switches.

be improved through tuning, though in doing so, one loses any convergence and optimality guarantees of the EKF.

The primary difference between the approach developed in this paper and the EKF is that our approach yields guarantees on estimation error convergence due to considering the full, inherently nonlinear dynamics of the image-based range estimation problem, whereas the EKF relies on linearization, and therefore can only yield local convergence guarantees, at best. Through the nonlinear Lyapunov analysis, an exponential convergence

envelope is developed, hence the fast convergence compared to the EKF. Since the EKF may only yield local convergence, it may not converge at all in certain instances, i.e., with large initial errors. As shown in the experimental results, even though the observer is initialized with a larger initial error than the EKF, the convergence is still faster than the EKF, despite the fact that the exponential envelope, and hence the convergence time, is proportional to the norm of the initial error.

The experimental results also seem to indicate better noise rejection due to the better performance during the latter parts of the experiment, however this is most likely a product of the high gain tradeoff. High gains increase robustness to disturbances and yield faster convergence, but also amplify noise, leading to larger steady-state error. In general terms (since a direct comparison between gains in the implemented observer and covariance matrices in the EKF is not sensible), in this particular experiment, the measurement and model uncertainties may be yielding lesser “gains” in the EKF, resulting in slower convergence but better noise rejection. The noise rejection of our approach can be improved through gain scheduling, thus maintaining fast convergence while improving long-term tracking performance. It should also be noted that these experiments were performed using only one of the many observers available in the literature that can be “plugged in,” and for which the analysis in this paper applies (see Assumption 6); other implementations may yield improved performance.

VIII. CONCLUSION

An analysis was performed to demonstrate the robustness of a class of observers to intermittent loss of sensing. The analysis is applicable to any exponentially convergent, image-based observer. From signals generated via a known motion model of the object, a predictor is used in conjunction with the observer to provide state estimates during the periods when the object is not visible. The predictor also aids in the stability analysis by allowing the error growth to be bounded by an exponential function during the periods when the object is hidden. If measurement loss is uncontrollable, the average dwell time and total unstable activation time can be calculated and checked against (14) and (15) to verify the convergence of state estimates and therefore their accuracy. These conditions could also be used to relax trajectory constraints for camera motion. In our previous results that do not use a predictor (cf. [65]), the error that is bounded by a tangent function, with finite escape time, leading to hard constraints on the maximum allowable contiguous time measurements can remain unavailable. In contrast, the results in this paper lead to the more relaxed average dwell time and total activation time conditions in (14) and (15). Simulation results in Section VI confirm that the improvements in stability and performance the analyses suggest are a consequence of the use of a predictor as opposed to the ZOH approach.

Experiments were performed to demonstrate the stability and performance of the proposed estimator-predictor scheme in two common scenarios. The experimental results are compared to the theoretically developed bounds to elucidate how conservative Lyapunov analysis can be. In addition, an EKF is

implemented for the SfM problem as a comparison to the approach developed in this paper. An example of how a common observer design that only recovers partial states can be augmented for full-state estimation and therefore can be used during periods of target visibility is provided.

The novelty of the developed approach is the ability to reconstruct relative Euclidean measurements of a target viewed by intermittent camera observations using any exponentially convergent observer. This contribution is enabled by using switched systems methods to analyze the stability of the state estimate when constructed by switching between the observer and the predictor. However, the current predictor is limited to applications, where target velocity information is measurable or available, either directly or through a known motion model. Further investigation is required to circumvent this requirement, either by changing the predictor structure, or by learning a motion model online while the target is visible.

APPENDIX

In [6], an observer is designed for the unmeasurable state x_3 , whereas it is assumed the estimates for the first two states x_1 and x_2 are directly measurable. If this design were directly implemented, the state estimates may discontinuously jump whenever the target comes into view, violating the continuity assumption of Theorem 1. By using filtered measurements for the complete state estimate, the continuity assumption can be satisfied. The observer used in the experiments described in Section VII is a modified version of the observer in [6] and is defined by the update laws

$$\begin{aligned}\dot{\hat{x}}_1 &= h_1 \hat{x}_3 + p_1 + k_1 e_1 \\ \dot{\hat{x}}_2 &= h_2 \hat{x}_3 + p_2 + k_2 e_2 \\ \dot{\hat{x}}_3 &= -b_3 \hat{x}_3^2 - (x_1 \omega_2 - x_2 \omega_1) \hat{x}_3 - k_3 (h_1^2 + h_2^2) \hat{x}_3 \\ &\quad + k_3 h_1 (\hat{x}_1 - p_1) + k_3 h_2 (\hat{x}_2 - p_2) + h_1 e_1 + h_2 e_2\end{aligned}$$

where the error signals, $\mathbf{e} \triangleq [e_1 \ e_2 \ e_3]^T \in \mathbb{R}^3$, are defined as

$$\begin{aligned}e_1 &\triangleq x_1 - \hat{x}_1, \\ e_2 &\triangleq x_2 - \hat{x}_2, \\ e_3 &\triangleq x_3 - \hat{x}_3,\end{aligned}$$

the linear velocity signal is defined as $\mathbf{b} \triangleq v_q - v_c \in \mathbb{R}^3$, $k_1, k_2, k_3 \in \mathbb{R}$ are positive constants, and the auxiliary signals $h_1, h_2, p_1, p_2 \in \mathbb{R}$ are defined

$$\begin{aligned}h_1 &\triangleq b_1 - x_1 b_3, \\ h_2 &\triangleq b_2 - x_2 b_3, \\ p_1 &\triangleq x_1 x_2 \omega_1 - (1 + x_1^2) \omega_2 + x_2 \omega_3, \\ p_2 &\triangleq (1 + x_2^2) \omega_1 - x_1 x_2 \omega_2 - x_1 \omega_3.\end{aligned}$$

Using the Lyapunov function candidate

$$V = \frac{1}{2} e_1^2 + \frac{1}{2} e_2^2 + \frac{1}{2} e_3^2$$

it can be shown that

$$\dot{V} \leq -k_1 e_1^2 - k_2 e_2^2 - k_4 e_3^2$$

for some positive constant $k_4 \in \mathbb{R}$, using the same bounding arguments and gain conditions as in [6]. Thus, the augmented observer is exponentially convergent.

ACKNOWLEDGMENT

Any opinions, findings, and conclusions or recommendations expressed in this material are those of the author(s) and do not necessarily reflect the views of the sponsoring agency.

REFERENCES

- [1] D. Braganza, D. M. Dawson, and T. Hughes, "Euclidean position estimation of static features using a moving camera with known velocities," in *Proc. IEEE Conf. Decision Control*, New Orleans, LA, USA, Dec. 2007, pp. 2695–2700.
- [2] O. Dahl, Y. Wang, A. F. Lynch, and A. Heyden, "Observer forms for perspective systems," *Automatica*, vol. 46, no. 11, pp. 1829–1834, Nov. 2010.
- [3] N. Zarrouati, E. Aldea, and P. Rouchon, "So(3)-invariant asymptotic observers for dense depth field estimation based on visual data and known camera motion," in *Proc. Amer. Control Conf.*, Montreal, QC, Canada, Jun. 2012, pp. 4116–4123.
- [4] A. Chiuso, P. Favaro, H. Jin, and S. Soatto, "Structure from motion causally integrated over time," *IEEE Trans. Pattern Anal. Mach. Intell.*, vol. 24, no. 4, pp. 523–535, Apr. 2002.
- [5] R. Spica, P. R. Giordano, and F. Chaumette, "Active structure from motion: Application to point, sphere, and cylinder," *IEEE Trans. Robot.*, vol. 30, no. 6, pp. 1499–1513, Dec. 2014.
- [6] A. Dani, N. Fischer, Z. Kan, and W. E. Dixon, "Globally exponentially stable observer for vision-based range estimation," *Mechatronics*, vol. 22, no. 4, pp. 381–389, 2012.
- [7] W. E. Dixon, Y. Fang, D. M. Dawson, and T. J. Flynn, "Range identification for perspective vision systems," *IEEE Trans. Autom. Control*, vol. 48, no. 12, pp. 2232–2238, Dec. 2003.
- [8] D. Karagiannis and A. Astolfi, "A new solution to the problem of range identification in perspective vision systems," *IEEE Trans. Autom. Control*, vol. 50, no. 12, pp. 2074–2077, Dec. 2005.
- [9] X. Chen and H. Kano, "A new state observer for perspective systems," *IEEE Trans. Autom. Control*, vol. 47, no. 4, pp. 658–663, Apr. 2002.
- [10] L. Ma, C. Cao, N. Hovakimyan, C. Woolsey, and W. E. Dixon, "Fast estimation and range identification in the presence of unknown motion parameters," *IMA J. Appl. Math.*, vol. 75, no. 2, pp. 165–189, 2010.
- [11] G. Hu, D. Aiken, S. Gupta, and W. Dixon, "Lyapunov-based range identification for a paracatadioptric system," *IEEE Trans. Autom. Control*, vol. 53, no. 7, pp. 1775–1781, Aug. 2008.
- [12] X. Chen and H. Kano, "State observer for a class of nonlinear systems and its application to machine vision," *IEEE Trans. Autom. Control*, vol. 49, no. 11, pp. 2085–2091, Nov. 2004.
- [13] A. Dani, Z. Kan, N. Fischer, and W. E. Dixon, "Structure and motion estimation of a moving object using a moving camera," in *Proc. Amer. Control Conf.*, Baltimore, MD, USA, 2010, pp. 6962–6967.
- [14] A. Dani, N. Fischer, and W. E. Dixon, "Single camera structure and motion," *IEEE Trans. Autom. Control*, vol. 57, no. 1, pp. 241–246, Jan. 2012.
- [15] M. Sznaier and O. Camps, "Motion prediction for continued autonomy," in *Encyclopedia of Complexity and Systems Science*. New York, NY, USA: Springer, 2009, pp. 5702–5718.
- [16] M. Sznaier, O. Camps, N. Ozay, T. Ding, G. Tadmor, and D. Brooks, "The role of dynamics in extracting information sparsely encoded in high dimensional data streams," in *Dynamics of Information Systems*, vol. 40. New York, NY, USA: Springer, 2010, pp. 1–27.
- [17] M. Yang, Y. Wu, and G. Hua, "Context-aware visual tracking," *IEEE Trans. Pattern Anal. Mach. Intell.*, vol. 31, no. 7, pp. 1195–1209, Jul. 2009.
- [18] H. Grabner, J. Matas, L. V. Gool, and P. Cattin, "Tracking the invisible: Learning where the object might be," in *Proc. IEEE Conf. Comput. Vision Pattern Recognit.*, San Francisco, CA, USA, Jun. 2010, pp. 1285–1292.

- [19] L. Cerman, J. Matas, and V. Hlavac, "Sputnik tracker: Having a companion improves robustness of the tracker," in *Proc. Scand. Conf.*, Oslo, Norway, Jun. 2009, pp. 291–300.
- [20] B. R. Fransen, O. I. Camps, and M. Sznaier, "Robust structure from motion and identified dynamics," in *Proc. IEEE Int. Conf. Comput. Vision*, Oct. 2005, pp. 772–777.
- [21] H. Durrant-Whyte and T. Bailey, "Simultaneous localization and mapping: Part I," *IEEE Robot. Autom. Mag.*, vol. 13, no. 2, pp. 99–110, Jun. 2006.
- [22] T. Bailey and H. Durrant-Whyte, "Simultaneous localization and mapping (SLAM): Part II," *IEEE Robot. Autom. Mag.*, vol. 13, no. 3, pp. 108–117, Sep. 2006.
- [23] M. W. M. G. Dissanayake, P. Newman, S. Clark, H. F. Durrant-Whyte, and M. Csorba, "A solution to the simultaneous localization and map building (SLAM) problem," *IEEE Trans. Robot. Autom.*, vol. 17, no. 3, pp. 229–241, Jun. 2001.
- [24] G. P. Huang, A. I. Mourikis, and S. I. Roumeliotis, "A quadratic-complexity observability-constrained unscented Kalman filter for SLAM," *IEEE Trans. Robot.*, vol. 29, no. 5, pp. 1226–1243, Oct. 2013.
- [25] J. Sola, A. Monin, M. Devy, and T. Vidal-Calleja, "Fusing monocular information in multicamera SLAM," *IEEE Trans. Robot.*, vol. 24, no. 5, pp. 958–968, Oct. 2008.
- [26] J. A. Hesch, D. G. Kottas, S. L. Bowman, and S. I. Roumeliotis, "Consistency analysis and improvement of vision-aided inertial navigation," *IEEE Trans. Robot.*, vol. 30, no. 1, pp. 158–176, Feb. 2014.
- [27] T. Lupton and S. Sukkari, "Visual-inertial-aided navigation for high-dynamic motion in built environments without initial conditions," *IEEE Trans. Robot.*, vol. 28, no. 1, pp. 61–76, Feb. 2012.
- [28] M. Kaess, A. Ranganathan, and F. Dellaert, "iSAM: Incremental smoothing and mapping," *IEEE Trans. Robot.*, vol. 24, no. 6, pp. 1365–1378, Dec. 2008.
- [29] M. Montemerlo, S. Thrun, D. Koller, and B. Wegbreit, "FastSLAM 2.0: An improved particle filtering algorithm for simultaneous localization and mapping that provably converges," in *Proc. Int. Joint Conf. Artif. Intell.*, 2003, pp. 1151–1156.
- [30] G. Grisetti, C. Stachniss, and W. Burgard, "Improved techniques for grid mapping with Rao-Blackwellised particle filters," *IEEE Trans. Robot.*, vol. 23, no. 1, pp. 34–46, Feb. 2007.
- [31] E. Mazor, A. Averbuch, Y. Bar-Shalom, and J. Dayan, "Interacting multiple model methods in target tracking: A survey," *IEEE Trans. Aerosp. Electron. Syst.*, vol. 34, no. 1, pp. 103–123, Jan. 1998.
- [32] S. S. Blackman, *Multiple-Target Tracking With Radar Applications*. Norwood, MA, USA: Artech House, 1986.
- [33] K. Granstrom and U. Orguner, "A PHD filter for tracking multiple extended targets using random matrices," *IEEE Trans. Signal Process.*, vol. 60, no. 11, pp. 5657–5671, Nov. 2012.
- [34] K. Wyffels and M. Campbell, "Negative observations for multiple hypothesis tracking of dynamic extended objects," in *Proc. Amer. Control Conf.*, 2014, pp. 642–647.
- [35] K. Wyffels and M. Campbell, "Negative information for occlusion reasoning in dynamic extended multiobject tracking," *IEEE Trans. Robot.*, vol. 31, no. 2, pp. 425–442, Apr. 2015.
- [36] A. Andriyenko, S. Roth, and K. Schindler, "An analytical formulation of global occlusion reasoning for multi-target tracking," in *Proc. IEEE Int. Conf. Comput. Vision Workshop*, 2011, pp. 1839–1846.
- [37] J. Liang, Z. Wang, and X. Liu, "Distributed state estimation for discrete-time sensor networks with randomly varying nonlinearities and missing measurements," *IEEE Trans. Neural Netw.*, vol. 22, no. 3, pp. 486–496, Mar. 2011.
- [38] L. Ma, F. Da, and K.-J. Zhang, "Exponential H_∞ filter design for discrete time-delay stochastic systems with Markovian jump parameters and missing measurements," *IEEE Trans. Circuits Syst.*, vol. 58, no. 5, pp. 994–1007, May 2011.
- [39] J. Hu, Z. Wang, H. Gao, and L. K. Stergioulas, "Extended Kalman filtering with stochastic nonlinearities and multiple missing measurements," *Automatica*, vol. 48, no. 9, pp. 2007–2015, Sep. 2012.
- [40] X. Yao, L. Wu, and W. X. Zheng, "Fault detection filter design for Markovian jump singular systems with intermittent measurements," *IEEE Trans. Signal Process.*, vol. 59, no. 7, pp. 3099–3109, Jul. 2011.
- [41] Y. Zhao, J. Lam, and H. Gao, "Fault detection for fuzzy systems with intermittent measurements," *IEEE Trans. Fuzzy Syst.*, vol. 17, no. 2, pp. 398–410, Apr. 2009.
- [42] J. You and S. Yin, " H_∞ filtering for time-delay T-S fuzzy systems with intermittent measurements and quantization," *J. Franklin Inst.*, vol. 351, pp. 3734–3751, Feb. 2013.
- [43] Z. Wang, B. Shen, and X. Liu, " H_∞ filtering with randomly occurring sensor saturations and missing measurements," *Automatica*, vol. 48, no. 3, pp. 556–562, Mar. 2012.
- [44] H. Gao, Y. Zhao, J. Lam, and K. Chen, " H_∞ fuzzy filtering of nonlinear systems with intermittent measurements," *IEEE Trans. Fuzzy Syst.*, vol. 17, no. 2, pp. 291–300, Apr. 2009.
- [45] S. Dey, A. S. Leong, and J. S. Evans, "Kalman filtering with faded measurements," *Automatica*, vol. 45, no. 10, pp. 2223–2233, Oct. 2009.
- [46] B. Sinopoli, L. Schenato, M. Franceschetti, K. Poolla, M. Jordan, and S. Sastry, "Kalman filtering with intermittent observations," *IEEE Trans. Autom. Control*, vol. 49, no. 9, pp. 1453–1464, Sep. 2004.
- [47] K. You, M. Fu, and L. Xie, "Mean square stability for Kalman filtering with Markovian packet losses," *Automatica*, vol. 47, no. 12, pp. 2647–2657, Dec. 2011.
- [48] H. Zhang and Y. Shi, "Observer-based H_∞ feedback control for arbitrarily time-varying discrete-time systems with intermittent measurements and input constraints," *J. Dyn. Syst. Meas. Control*, vol. 134, no. 6, Sep. 2012, Art. no. 061008.
- [49] B. Shen, Z. Wang, H. Shu, and G. Wei, "On nonlinear H_∞ filtering for discrete-time stochastic systems with missing measurements," *IEEE Trans. Autom. Control*, vol. 53, no. 9, pp. 2170–2180, Oct. 2008.
- [50] S. C. Smith and P. Seiler, "Optimal pseudo-steady-state estimators for systems with Markovian intermittent measurements," in *Proc. Amer. Control Conf.*, 2002, vol. 4, pp. 3021–3027.
- [51] H. M. Faridani, "Performance of Kalman filter with missing measurements," *Automatica*, vol. 22, no. 1, pp. 117–120, 1986.
- [52] L. K. Carvalho, J. C. Basilio, and M. V. Moreira, "Robust diagnosis of discrete event systems against intermittent loss of observations," *Automatica*, vol. 48, no. 9, pp. 2068–2078, 2012.
- [53] J. You, S. Yin, and H. R. Karimi, "Robust estimation for discrete Markov system with time-varying delay and missing measurements," *Math. Probl. Eng.*, vol. 2013, 2013, Art ID: 321935.
- [54] Z. Wang, F. Yang, D. W. C. Ho, and X. Liu, "Robust finite-horizon filtering for stochastic systems with missing measurements," *IEEE Signal Process. Lett.*, vol. 12, no. 6, pp. 437–440, Jun. 2005.
- [55] Z. Wang, D. W. Ho, Y. Liu, and X. Liu, "Robust H_∞ control for a class of nonlinear discrete time-delay stochastic systems with missing measurements," *Automatica*, vol. 45, no. 3, pp. 684–691, 2009.
- [56] Z. Wang, F. Yang, D. W. Ho, and X. Liu, "Robust H_∞ filtering for stochastic time-delay systems with missing measurements," *IEEE Trans. Signal Process.*, vol. 54, no. 7, pp. 2579–2587, Jul. 2006.
- [57] F. O. Hounkpevi and E. E. Yaz, "Robust minimum variance linear state estimators for multiple sensors with different failure rates," *Automatica*, vol. 43, no. 7, pp. 1274–1280, 2007.
- [58] H. Liang and T. Zhou, "Robust state estimation for uncertain discrete-time stochastic systems with missing measurements," *Automatica*, vol. 47, no. 7, pp. 1520–1524, 2011.
- [59] L. Ma, Z. Wang, J. Hu, Y. Bo, and Z. Guo, "Robust variance-constrained filtering for a class of nonlinear stochastic systems with missing measurements," *Signal Process.*, vol. 90, no. 6, pp. 2060–2071, Jun. 2010.
- [60] J. Liang, Z. Wang, and X. Liu, "State estimation for coupled uncertain stochastic networks with missing measurements and time-varying delays: The discrete-time case," *IEEE Trans. Neural Netw.*, vol. 20, no. 5, pp. 781–793, May 2009.
- [61] S. Kluge, K. Reif, and M. Brokate, "Stochastic stability of the extended Kalman filter with intermittent observations," *IEEE Trans. Autom. Control*, vol. 55, no. 2, pp. 514–518, Feb. 2010.
- [62] L. Li and Y. Xia, "Stochastic stability of the unscented Kalman filter with intermittent observations," *Automatica*, vol. 48, no. 5, pp. 978–981, 2012.
- [63] S. Deshmukh, B. Natarajan, and A. Pahwa, "Stochastic state estimation for smart grids in the presence of intermittent measurements," in *Proc. IEEE Latin Amer. Conf. Commun.*, 2012, pp. 1–6.
- [64] Z. Wang, D. W. Ho, and X. Liu, "Variance-constrained filtering for uncertain stochastic systems with missing measurements," *IEEE Trans. Autom. Control*, vol. 48, no. 7, pp. 1254–1258, Jul. 2003.
- [65] A. Parikh, T.-H. Cheng, and W. E. Dixon, "A switched systems approach to image-based localization of targets that temporarily leave the field of view," in *Proc. IEEE Conf. Decision Control*, 2014, pp. 2185–2190.
- [66] A. Parikh, T.-H. Cheng, and W. E. Dixon, "A switched systems approach to vision-based localization of a target with intermittent measurements," in *Proc. Amer. Control Conf.*, Jul. 2015, pp. 4443–4448.
- [67] F. Chaumette and S. Hutchinson, "Visual servo control part I: Basic approaches," *IEEE Robot. Autom. Mag.*, vol. 13, no. 4, pp. 82–90, Dec. 2006.

- [68] S. S. Mehta, T. Burks, and W. E. Dixon, "A theoretical model for vision-based localization of a wheeled mobile robot in greenhouse applications: A daisy chaining approach," *Comput. Electron. Agriculture*, vol. 63, pp. 28–37, 2008.
- [69] K. Dupree, N. R. Gans, W. MacKunis, and W. E. Dixon, "Euclidean calculation of feature points of a rotating satellite: A daisy chaining approach," *AIAA J. Guid. Control Dyn.*, vol. 31, pp. 954–961, 2008.
- [70] R. Sharma, S. Quebe, R. W. Beard, and C. N. Taylor, "Bearing-only cooperative localization," *J. Intell. Robot. Syst.*, vol. 72, nos. 3/4, pp. 429–440, Dec. 2013.
- [71] S. I. Roumeliotis and G. A. Bekey, "Distributed multirobot localization," *IEEE Trans. Robot. Autom.*, vol. 18, no. 5, pp. 781–795, Oct. 2002.
- [72] A. I. Mourikis and S. I. Roumeliotis, "Performance analysis of multirobot cooperative localization," *IEEE Trans. Robot.*, vol. 22, no. 4, pp. 666–681, Aug. 2006.
- [73] X. S. Zhou and S. I. Roumeliotis, "Robot-to-robot relative pose estimation from range measurements," *IEEE Trans. Robot.*, vol. 24, no. 6, pp. 1379–1393, Dec. 2008.
- [74] Y. Ma, S. Soatto, J. Kosecka, and S. Sastry, *An Invitation to 3-D Vision*. New York, NY, USA: Springer, 2004.
- [75] P. Corke, *Robotics, Vision and Control*, 1st ed. (Springer Tracts in Advanced Robotics), B. Siciliano and O. Khatib, Eds. Berlin, Germany: Springer, 2011.
- [76] C. Tomasi and T. Kanade, "Detection and tracking of point features," Carnegie Mellon Univ., Pittsburgh, PA, USA, *Tech. Rep. CMU-CS-91-132*, Apr. 1991.
- [77] D. Lowe, "Distinctive image features from scale-invariant keypoints," *Int. J. Comput. Vision*, vol. 60, pp. 91–110, 2004.
- [78] H. Bay, A. Ess, T. Tuytelaars, and L. Van Gool, "Speeded-up robust features (surf)," *Comput. Vision Image Underst.*, vol. 110, no. 3, pp. 346–359, 2008.
- [79] O. Russakovsky *et al.*, "Imagenet large scale visual recognition challenge," *Int. J. Comput. Vision*, 2015, pp. 1–42.
- [80] Z. Kalal, K. Mikolajczyk, and J. Matas, "Tracking-learning-detection," *IEEE Trans. Pattern Anal. Mach. Intell.*, vol. 34, no. 7, pp. 1409–1422, Jul. 2012.
- [81] T. Tuytelaars and K. Mikolajczyk, *Local Invariant Feature Detectors: A Survey (Foundations and Trends in Computer Graphics and Vision)*. Delft, The Netherlands: Now Publishers Inc, 2008.
- [82] A. Yilmaz, O. Javed, and M. Shah, "Object tracking: A survey," *ACM Comput. Surv.*, vol. 38, no. 4, pp. 1–45, 2006.
- [83] M. Krstic, I. Kanellakopoulos, and P. V. Kokotovic, *Nonlinear and Adaptive Control Design*. New York, NY, USA: Wiley, 1995.
- [84] W. E. Dixon, A. Behal, D. M. Dawson, and S. Nagarkatti, *Nonlinear Control of Engineering Systems: A Lyapunov-Based Approach*. Boston, MA, USA: Birkhauser, 2003.
- [85] A. Dani, Z. Kan, N. Fischer, and W. E. Dixon, "Structure estimation of a moving object using a moving camera: An unknown input observer approach," in *Proc. IEEE Conf. Decision Control*, Orlando, FL, USA, 2011, pp. 5005–5012.
- [86] A. De Luca, G. Oriolo, and P. Robuffo Giordano, "Feature depth observation for image-based visual servoing: Theory and experiments," *Int. J. Robot. Res.*, vol. 27, no. 10, pp. 1093–1116, 2008.
- [87] F. Morbidi and D. Prattichizzo, "Range estimation from a moving camera: An immersion and invariance approach," in *Proc. IEEE Int. Conf. Robot. Autom.*, Kobe, Japan, May 2009, pp. 2810–2815.
- [88] J. P. Hespanha and A. S. Morse, "Stability of switched systems with average dwell-time," in *Proc. IEEE Conf. Decision Control*, Dec. 1999, pp. 2655–2660.
- [89] M. A. Müller and D. Liberzon, "Input/output-to-state stability and state-norm estimators for switched nonlinear systems," *Automatica*, vol. 48, no. 9, pp. 2029–2039, 2012.
- [90] H. K. Khalil, *Nonlinear Systems*, 3rd ed. Upper Saddle River, NJ, USA: Prentice-Hall, 2002.
- [91] S. Garrido-Jurado, R. Muñoz-Salinas, F. Madrid-Cuevas, and M. Marín-Jiménez, "Automatic generation and detection of highly reliable fiducial markers under occlusion," *Pattern Recognit.*, vol. 47, no. 6, pp. 2280–2292, Jun. 2014.
- [92] Aruco library. (2015). [Online]. Available: <http://www.uco.es/investig/grupos/ava/node/26>



Anup Parikh received the B.S. degree in mechanical and aerospace engineering, the M.S. degree in mechanical engineering, and the Ph.D. degree in aerospace engineering from University of Florida, Gainesville, FL, USA.

He is a Postdoctoral Researcher in Sandia National Laboratories, Albuquerque, NM, USA. His primary research interests include Lyapunov-based control and estimation theory and application in autonomous systems.



Teng-Hu Cheng received the Ph.D. degree in mechanical engineering from the Department of Mechanical Engineering, University of Florida, Gainesville, FL, USA, in 2015, under the supervision of Dr. Warren Dixon.

In 2016, he joined the Department of Mechanical Engineering, National Chiao Tung University, Hsinchu, Taiwan. His research interests include networked system control, switched control, event-driven control, and nonlinear control.



Hsi-Yuan Chen received the Bachelor of Science degree in mechanical engineering from the Mechanical Engineering Department, National Taiwan University of Science and Technology, Taipei, Taiwan, in 2014. He is currently working toward the doctoral degree at University of Florida, Gainesville, FL, USA, under the supervision of Dr. Dixon.

As an undergraduate, he joined the Center for Intelligent Robots, where he spent two years researching robotic vision and navigation theories. His primary research interests include simultaneous localization and mapping, object recognition, and other vision-based control systems.

calization and mapping, object recognition, and other vision-based control systems.



Warren E. Dixon (F'15) received the Ph.D. degree in electrical engineering from the Department of Electrical and Computer Engineering, Clemson University, Clemson, SC, USA, in 2000.

In 2004, he joined the Mechanical and Aerospace Engineering Department, University of Florida, Gainesville, FL, USA. His main research interests include the development and application of Lyapunov-based control techniques for uncertain nonlinear systems. He has published 3 books, an edited collection, 13 chapters, and more than 130 journal and 230 conference papers.

Dr. Dixon was selected as an Eugene P. Wigner Fellow at Oak Ridge National Laboratory (ORNL). He received the 2015 & 2009 American Automatic Control Council O. Hugo Schuck (Best Paper) Award, the 2013 Fred Ellersick Award for Best Overall MILCOM Paper, a 2012–2013 University of Florida College of Engineering Doctoral Dissertation Mentoring Award, the 2011 American Society of Mechanical Engineers (ASME) Dynamics Systems and Control Division Outstanding Young Investigator Award, the 2006 IEEE Robotics and Automation Society Early Academic Career Award, an NSF CAREER Award (2006–2011), the 2004 Department of Energy Outstanding Mentor Award, and the 2001 ORNL Early Career Award for Engineering Achievement. He is an ASME Fellow, an IEEE Control Systems Society (CSS) Distinguished Lecturer, and served as the Director of Operations for the Executive Committee of the IEEE CSS Board of Governors (2012–2015). He currently serves as a member of the U.S. Air Force Science Advisory Board. He is currently or formerly an Associate Editor of *ASME Journal of Journal of Dynamic Systems, Measurement and Control*, *Automatica*, *IEEE TRANSACTIONS ON SYSTEMS MAN AND CYBERNETICS: PART B CYBERNETICS*, and *International Journal of Robust and Nonlinear Control*.